

Sweeping across the BCS-BEC crossover, reentrant, and hidden quantum phase transitions in two-band superconductors by tuning the valence and conduction bands

Giovanni Midei¹ and Andrea Perali²¹*School of Science and Technology, Physics Division, University of Camerino, Via Madonna delle Carceri, 9B, 62032–Camerino (MC), Italy*²*School of Pharmacy, Physics Unit, University of Camerino, Via Madonna delle Carceri, 9B, 62032–Camerino (MC), Italy*

(Received 31 January 2023; revised 4 April 2023; accepted 18 April 2023; published 2 May 2023)

Two-band electronic structures with a valence and a conduction band separated by a tunable energy gap and with pairing of electrons in different channels can be relevant to investigate the properties of two-dimensional multiband superconductors and electron-hole superfluids, such as monolayer FeSe, recently discovered superconducting bilayer graphene, and double-bilayer graphene electron-hole systems. This electronic configuration also allows us to study the coexistence of superconductivity and charge-density waves in connection with underdoped cuprates and transition metal dichalcogenides. By using a mean-field approach to study the system mentioned above, we have obtained numerical results for superconducting gaps, chemical potential, condensate fractions, coherence lengths, and superconducting mean-field critical temperature, considering a tunable band gap and different fillings of the conduction band, for a parametric choice of the pairing interactions. By tuning these quantities, the electrons redistribute among valence and conduction band in a complex way, leading to a new physics with respect to single-band superconductors, such as density-induced and band-selective BCS-BEC crossover, quantum phase transitions, and hidden criticalities. At finite temperature, this phenomenon is also responsible for the nonmonotonic behavior of the superconducting gaps resulting in a superconducting-normal state reentrant transition, without the need of disorder or magnetic effects.

DOI: [10.1103/PhysRevB.107.184501](https://doi.org/10.1103/PhysRevB.107.184501)

I. INTRODUCTION

Multiband and multigap superconductivity is a complex quantum coherent phenomenon with peculiar features that cannot be found in single-band and single-gap superconductors [1]. The increased number of degrees of freedom in the condensate state allows for unique quantum effects which are unattainable otherwise, for instance, enriching the physics of the BCS-BEC crossover [2–5]. Proximity to the crossover regime of the BCS-BEC crossover in multiband superconductors having deep and shallow bands can determine a notable increase of superconducting gaps and critical temperature (T_c) [6–9], associated with a higher mean-field T_c , together with optimal conditions for the screening of superconducting fluctuations [10–12]. Furthermore, the interplay of low-dimensional two-band systems allows for screening of fluctuations in systems composed by coupled quasi-two-dimensional bands or even in the vicinity of a van Hove singularity (e.g., in the case of quasi-one-dimensional), enabling shrinking of the pseudogap phase and robust high-critical temperatures [13–15].

Motivated by high-temperature superconductivity and anomalous metallic-state properties in underdoped cuprates, interest has grown in the pseudogap physics, in which a blurred gap persists in the normal state near the Fermi level. There are different models and explanations for this pseudogap, the simplest one being a smooth crossover from the BCS regime towards a Bose-Einstein condensation regime in which bound pairs form first at higher temperatures, and then below a critical temperature T_c they condense, with the

pseudogap being the excitation energy of the quasimolecular pairs. Another explanation relevant for underdoped cuprates is the presence of other mechanisms different from pair fluctuations, such as charge density waves (CDWs) [16–19] and their fluctuations that can modify the energy spectrum with opening of (pseudo)gaps and at the same time mediate Cooper pairing. Thus, systems in which CDWs and superconductivity coexist are of primary interest to study the BCS-BEC crossover when an energy gap separates the electronic spectrum in two bands. The CDW instability or its precursor opens a gap or a pseudogap at low energies, splitting the single band of the nonordered state in two branches that in wave-vector space behave locally as valence (holelike) and conduction (electronlike) bands, characterized by an energy separation that is twice the gap or pseudogap energy.

In addition to underdoped cuprates, an interesting example is given by the transition metal dichalcogenide family, MX_2 , where $M = \text{Ti, Nb, Mo, Ta}$ and $X = \text{S, Se}$, which exhibits a rich interplay between superconductivity and CDW order [20]. In these materials, superconductivity occurs in an environment of pre-existing CDW order [21,22], making them an ideal platform to study many-body ground states and competing phases in the two-dimensional (2D) regime. The relationship between CDW and superconductivity in such systems is still under investigation [23,24]. In general, their mutual interaction is competitive, but evidence to the contrary, indicating a cooperative interplay, has also been reported in angle-resolved photoemission spectroscopy studies [22]. Among them, bulk Niobium diselenide (2H-NbSe_2) undergoes a CDW distortion at $T = 30$ K and becomes superconducting at 7 K.

References [25,26] reported that T_c lowers to 1.9 K in 2H-NbSe₂ single layers and that the CDW measured in the bulk is preserved. Theoretical support is given by Lian *et al.* [27]: They demonstrated enhanced superconductivity in the CDW state of monolayer tantalium diselenide (TaSe₂) with DFT calculations. In contrast with 2H-NbSe₂, they reported that as TaSe₂ is thinned to the monolayer limit, its superconducting critical temperature rises from 0.14 K in the bulk to 2 K in the monolayer. Another appealing superconducting material is the monolayer FeSe grown on a SrTiO₃ substrate, which exhibits a huge increase of T_c up to 100 K [28] and is characterized by a valence and conduction band structure near the Fermi level. Interestingly, spectroscopic evidence of a real-space BCS-BEC crossover in a FeSe monolayer by using spatially resolved scanning tunneling microscopy has been recently reported [29]. The BCS-BEC crossover in this system is driven by the shift of band structure relative to the Fermi level. Furthermore, very recently, 2D superconductivity has been found in bilayer graphene systems, in which conduction and valence bands are separated by a small energy band gap (0 ÷ 100 meV) that can be precisely tuned by an external electric field [30] (for a review, see Ref. [31]). Coupling a monolayer of WSe₂ with bilayer graphene has been found to enhance superconductivity by an order of magnitude in T_c and superconductivity emerges already at zero magnetic field [32]. Finally, it turns out that the two-band superconducting system considered in this paper is in close correspondence with two-band electron-hole superfluids in double bilayer graphene [33].

Therefore, the growing experimental realization of 2D superconductors with valence and conduction bands separated by a tunable energy gap and electron-hole superfluidity in multilayer systems motivated us to investigate the BCS-BEC crossover in this kind of system. The detailed analysis of this configuration is lacking in the literature to the best of our knowledge. A pioneering work on a related system with valence and conduction parabolic bands has been done by Nozières and Pistoletti [34] to study the phase transition from a semiconducting to a superconducting state and the consequent (pseudo)gap opening, in the specific case of equal pairing strengths for all interaction channels considered. In our paper, we consider a superconductor with two tight-binding bands with different intraband and pair-exchange couplings to probe the possibility to have coexisting Cooper pairs of different average sizes [35] in the valence and conduction band. However, for most multiband superconductors, the tuning of intraband and pair-exchange interactions is rather challenging and their properties cannot be studied easily in a continuous way across the BCS-BEC crossover. As shown in this paper, a different way to explore the BCS-BEC crossover in such systems can be achieved by tuning the energy gap between the valence and the conduction band. In fact, since the number of particles in the single bands is not conserved, when the energy band gap is modified, the number of holes and electrons forming Cooper pairs, respectively, in the valence and in the conduction bands changes, allowing for the occurrence of a density-induced multiband BCS-BEC crossover [36]. This redistribution of charges between the valence and conduction bands also leads to interesting quantum phase transitions (QPTs) from a superconducting to an insulating state, or hidden criticalities

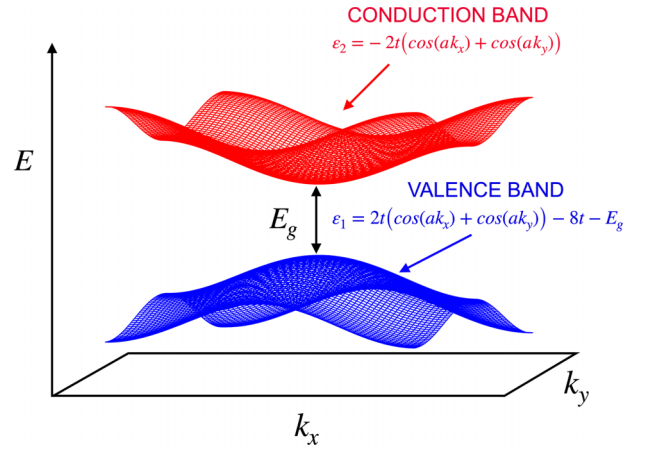


FIG. 1. Electronic band structure of the two-band 2D system considered in this paper. E_g is the energy gap between the valence ($i = 1$) and the conduction ($i = 2$) band.

evidenced by the analysis of the order parameter coherence lengths [37,38]. At finite temperature, a different type of reentrant superconducting to normal state transition has been also found and characterized. The results reported and discussed in this paper demonstrate the richness of the proposed valence and conduction band configuration to generate and tune unique types of crossover phenomena and quantum phases.

The paper is organized as follow. In Sec. II, we describe the model for the physical system considered and the theoretical approach for the evaluation of the superconducting state properties. In Sec. III, we report our results. The conclusions of our work will be reported in Sec. IV.

II. MODEL SYSTEM AND THEORETICAL APPROACH

We consider a 2D two-band superconductor with a valence and conduction electronic band in a square lattice. The valence and conduction bands are modeled by a tight-binding dispersion given, respectively, by Eqs. (1) and (2):

$$\varepsilon_1(\mathbf{k}) = 2t[\cos(k_x a) + \cos(k_y a)] - 8t - E_g, \quad (1)$$

$$\varepsilon_2(\mathbf{k}) = -2t[\cos(k_x a) + \cos(k_y a)], \quad (2)$$

where t is the nearest-neighbor hopping parameter assumed to be the same for both bands, a is the lattice parameter, and the wave vectors belong to the first Brillouin zone $-\frac{\pi}{a} \leq k_{x,y} \leq \frac{\pi}{a}$; E_g is the energy band gap between the conduction and the valence band. The energy band gap E_g considered in our model can simulate a well-formed pseudogap or a gap opening in the single-particle excitation spectrum in a family of correlated systems at high temperature, due to charge ordering instability or its precursor, and to study its effect on the superconducting state that arises at lower temperature. On the other hand, our two-band model can be relevant to study the superconducting properties of other two-dimensional systems in which E_g can be controlled, for example, by an external electric field. The band dispersions are reported in Fig. 1. To study the superconducting state properties of our system, we assume that Cooper pair formation is due to an attractive interaction between opposite spin electrons. The

two-particle interaction has been approximated by a separable potential $V_{ij}(\mathbf{k}, \mathbf{k}')$ with an energy cutoff ω_0 , which is given by

$$V_{ij}(\mathbf{k}, \mathbf{k}') = -V_{ij}^0 \Theta(\omega_0 - |\xi_i(\mathbf{k})|) \Theta(\omega_0 - |\xi_j(\mathbf{k}')|), \quad (3)$$

where $V_{ij}^0 > 0$ is the strength of the potential in the different pairing channels and i, j label the bands. V_{11}^0 and V_{22}^0 are the strengths of the intraband pairing interactions (Cooper pairs are created and destroyed in the same band). V_{12}^0 and V_{21}^0 are the strengths of the pair-exchange interactions (Cooper pairs are created in one band and destroyed in the other band, and vice versa), so superconductivity in one band can induce superconductivity in the other band. The same energy cutoff ω_0 of the interaction for intraband and pair-exchange terms is considered. Throughout this paper, ω_0 is considered an energy scale larger than the total bandwidth of our system to model an effective pairing of electronic origin or a contact attractive potential. This is a key assumption that makes it possible for the system to explore the entire BCS-BEC crossover [39]. The terms corresponding to Cooper pairs forming from electrons associated with different bands (interband or cross-band pairing) are not considered in this paper (see Ref. [40]). $\xi_i(\mathbf{k}) = \varepsilon_i(\mathbf{k}) - \mu$ in Eq. (3) is the energy dispersion for band i with respect to the chemical potential μ . The superconducting state of the system and its evolution with relevant system parameters is studied at a mean-field level. The BCS equations for the superconducting gaps have to be coupled with the density equation which fixes the chemical potential, since the self-consistent renormalization of the chemical potential is a key feature to account for the BCS-BEC crossover physics. Zero and finite temperature cases have been considered in this paper. The BCS equations for the superconducting gaps in the two-band system at a given temperature T are

$$\Delta_1(\mathbf{k}) = -\frac{1}{2\Omega} \sum_{\mathbf{k}'} \left[V_{11}(\mathbf{k}, \mathbf{k}') \frac{\Delta_1(\mathbf{k}')}{E_1(\mathbf{k}')} \tanh \frac{E_1(\mathbf{k}')}{2T} + V_{12}(\mathbf{k}, \mathbf{k}') \frac{\Delta_2(\mathbf{k}')}{E_2(\mathbf{k}')} \tanh \frac{E_2(\mathbf{k}')}{2T} \right], \quad (4)$$

$$\Delta_2(\mathbf{k}) = -\frac{1}{2\Omega} \sum_{\mathbf{k}'} \left[V_{22}(\mathbf{k}, \mathbf{k}') \frac{\Delta_2(\mathbf{k}')}{E_2(\mathbf{k}')} \tanh \frac{E_2(\mathbf{k}')}{2T} + V_{21}(\mathbf{k}, \mathbf{k}') \frac{\Delta_1(\mathbf{k}')}{E_1(\mathbf{k}')} \tanh \frac{E_1(\mathbf{k}')}{2T} \right], \quad (5)$$

where $E_i(\mathbf{k}) = \sqrt{\xi_i(\mathbf{k})^2 + \Delta_i(\mathbf{k})^2}$ is the dispersion of single-particle excitations in the superconducting state and Ω is the area occupied by the 2D system. $\hbar = 1$ and $k_B = 1$ throughout the paper. The superconducting gaps have the same energy cutoff of the separable interaction:

$$\Delta_i(\mathbf{k}) = \Delta_i \Theta(\omega_0 - |\xi_i(\mathbf{k})|). \quad (6)$$

The total electron density of the two-band system is fixed and given by the sum of the single-band densities, $n_{\text{tot}} = n_1 + n_2$, that can vary instead. The electronic density n_i in the band (i) at temperature T is given by

$$n_i = \frac{2}{\Omega} \sum_{\mathbf{k}} [v_i(\mathbf{k})^2 f(-E_i(\mathbf{k})) + u_i(\mathbf{k})^2 f(E_i(\mathbf{k}))], \quad (7)$$

where $f(E)$ is the Fermi-Dirac distribution function. The BCS coherence weights $v_i(\mathbf{k})$ and $u_i(\mathbf{k})$ are

$$v_i(\mathbf{k})^2 = \frac{1}{2} \left[1 - \frac{\xi_i(\mathbf{k})}{\sqrt{\xi_i(\mathbf{k})^2 + \Delta_i(\mathbf{k})^2}} \right], \quad (8)$$

$$u_i(\mathbf{k})^2 = 1 - v_i(\mathbf{k})^2. \quad (9)$$

The mean-field critical temperature of the phase transition T_c in the two-band superconductor under consideration is determined by imposing that both superconducting gaps Δ_1 and Δ_2 in Eqs. (4) and (5) vanish at the same T_c , resulting in the condition

$$\begin{vmatrix} a_{11} - 1 & a_{12} \\ a_{21} & a_{22} - 1 \end{vmatrix} = 0, \quad (10)$$

where

$$a_{ij} = -\frac{1}{\Omega} \sum_{\mathbf{k}'} \frac{V_{ij}(\mathbf{k}, \mathbf{k}')}{2\xi_j(\mathbf{k}')} \tanh \frac{\xi_j(\mathbf{k}')}{2T_c}. \quad (11)$$

To explore the BCS-BEC crossover and to determine its boundaries for a given set of parameters in our system, we evaluate the condensate fraction, that can be used for this purpose when the BEC regime of the BCS-BEC crossover corresponds to a system of bosons with a weak residual mutual interaction, in such a way to not have the depletion of the condensate caused by boson-boson repulsive interactions. The validity of the condensate fraction as a detection parameter for the BCS-BEC crossover has been tested in Ref. [39], comparing the crossover boundaries \hat{A} obtained with the intrapair correlation length (the average pair size) and the ratio between the superconducting gap energy and the Fermi energy. Furthermore, similar conclusions have been obtained with the quantitative comparisons between quantum Monte Carlo simulations and mean-field predictions in Refs. [41,42], where it is reported that the low-density regime (that we are considering in our paper) allows us to minimize the effects of the dipolar interactions among the bosons, leading to a condensed fraction of order unity in the BEC regime. For the valence band, the definition of the condensate fraction is the ratio of the number of Cooper pairs in the valence band to the number of holes in the valence band:

$$\alpha_1^h = \frac{\sum_{\mathbf{k}} (u_1(\mathbf{k})v_1(\mathbf{k}))^2}{\sum_{\mathbf{k}} u_1(\mathbf{k})^2}. \quad (12)$$

For the conduction band instead, the expression already used in the one-band case is generalized to the number of Cooper pairs divided by the total number of carriers in the conduction band:

$$\alpha_2^e = \frac{\sum_{\mathbf{k}} (u_2(\mathbf{k})v_2(\mathbf{k}))^2}{\sum_{\mathbf{k}} v_2(\mathbf{k})^2}. \quad (13)$$

The intrapair coherence length ξ_{pair_i} has the same form for both the valence and the conduction bands, that is,

$$\xi_{\text{pair}_i}^2 = \frac{\sum_{\mathbf{k}} |\nabla(u_i(\mathbf{k})v_i(\mathbf{k}))|^2}{\sum_{\mathbf{k}} (u_i(\mathbf{k})v_i(\mathbf{k}))^2}. \quad (14)$$

Regarding the superconducting order parameter coherence length, two characteristic length scales in the spatial behavior of superconducting fluctuations are expected, since the system is made up by two partial condensates. When the

pair-exchange interaction is not present, these two lengths are simply the order parameter coherence lengths of the condensates of the valence ξ_{c1} and the conduction ξ_{c2} band. When the pair-exchange interaction is different from zero, one has to deal with coupled condensates, and these length scales cannot be attributed to the single bands involved, describing instead the collective features of the whole two-component condensate. The pair-exchange interactions mix the superconducting order parameters of the initially noninteracting bands that acquire mixed character. The soft, or critical, coherence length ξ_s diverges at the phase transition point, while the rigid, or noncritical, coherence length ξ_r remains finite. Following the approach in Ref. [38], these characteristic length scales are given by

$$\xi_{s,r}^2 = \frac{G(T) \pm \sqrt{G^2(T) - 4K(T)\gamma(T)}}{2K(T)}, \quad (15)$$

where ξ_s corresponds to the solution with the plus and ξ_r to the one with the minus sign and

$$\begin{aligned} G(T) = & (V_{12}^0)^2 (\tilde{g}_1(T)\beta_2(T) + \tilde{g}_2(T)\beta_1(T)) \\ & + (1 - V_{11}^0 \tilde{g}_1(T)) V_{22}^0 \beta_2(T) \\ & + (1 - V_{22}^0 \tilde{g}_2(T)) V_{11}^0 \beta_1(T), \end{aligned} \quad (16)$$

$$K(T) = (1 - V_{11}^0 \tilde{g}_1(T))(1 - V_{22}^0 \tilde{g}_2(T)) - (V_{12}^0)^2 \tilde{g}_1(T) \tilde{g}_2(T), \quad (17)$$

$$\gamma(T) = (V_{11}^0 V_{22}^0 - (V_{12}^0)^2) \beta_1(T) \beta_2(T), \quad (18)$$

$$\tilde{g}_i(T) = g_i(T) - 3v_i(T)(\Delta_i(T))^2, \quad (19)$$

$$g_i(T) = \frac{1}{2\Omega} \sum_{\mathbf{k}} \frac{1}{\xi_i(\mathbf{k})} \tanh \frac{\xi_i(\mathbf{k})}{2T}, \quad (20)$$

$$v_i(T) = -\frac{1}{2\Omega} \sum_{\mathbf{k}} \frac{\partial}{\partial |\Delta_i|^2} \left(\frac{1}{E_i(\mathbf{k})} \tanh \frac{\xi_i(\mathbf{k})}{2T} \right)_{\Delta_i=0}, \quad (21)$$

$$\begin{aligned} \beta_i(T) = & -\frac{1}{4\Omega} \sum_{\mathbf{k}} \frac{\partial^2}{\partial q_l^2} \left[\frac{1}{\xi_i(\mathbf{k}) + \xi_i(\mathbf{k} - \mathbf{q})} \right. \\ & \left. \times \left(\tanh \frac{\xi_i(\mathbf{k})}{2T} + \tanh \frac{\xi_i(\mathbf{k} - \mathbf{q})}{2T} \right) \right]_{\mathbf{q}=0}, \end{aligned} \quad (22)$$

where l refers to the Cartesian axis in Eq. (22).

To describe the physics of the quantum phase transition, the values of the coherence lengths at zero temperature have been approximated by choosing a low enough temperature so the superconducting gaps and the chemical potential retain the same behavior of the zero temperature case. The energies are normalized in units of the hopping t and the dimensionless couplings λ_{ii} are defined as $\lambda_{ii} = NV_{ii}^0$, where $N = 1/4\pi a^2 t$ is the density of states at the top/bottom of the valence/conduction band that coincide, since the density of states is not modified by the concavity of the band. The intrapair coherence lengths ξ_{pair_i} are normalized using the average interparticle distance in the normal state $l_i = 1/\sqrt{\pi n_i}$, where n_i is the density in the band i . These quantities differ by a factor of $\sqrt{2}$ by the inverse of the respective Fermi wave vector K_{Fi} . The soft ξ_s and the rigid ξ_r coherence lengths are

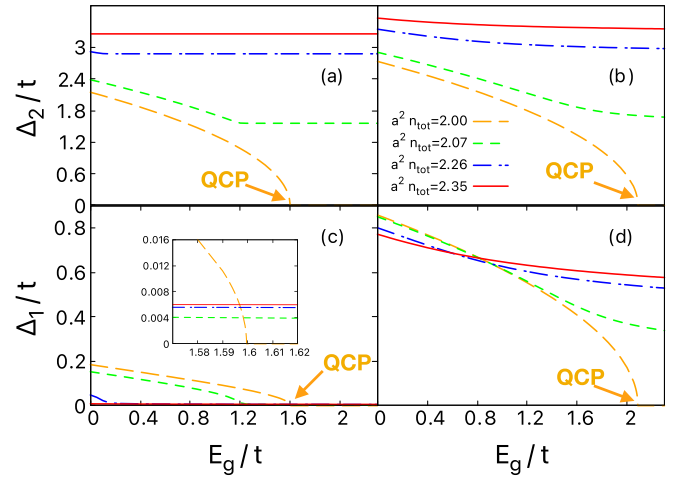


FIG. 2. Superconducting gaps Δ_2/t opening in the conduction band (a), (b) and in the valence band Δ_1/t (c), (d) as functions of the band gap energy E_g/t for an energy cutoff of the attractive interactions $\omega_0/t = 20$. The intraband couplings are $\lambda_{11} = 0.23$ and $\lambda_{22} = 0.75$. The pair-exchange couplings are ($\lambda_{12} = \lambda_{21}$): (a), (c) (0.001); (b), (d) (0.1). The superconducting gaps are reported for different values of the total density $a^2 n_{\text{tot}}$.

normalized with respect to the lattice constant a , since in the two-band case they cannot be attributed to either of the two bands.

III. RESULTS

In this section, we study the properties of the superconducting ground state and give a full characterization of the BCS-BEC crossover in the two-band system considered in this paper. First, we study the zero-temperature superconducting gaps in the conduction (Δ_2) and valence (Δ_1) band through the BCS-BEC crossover, for the case of unbalanced intraband couplings ($\lambda_{11} \neq \lambda_{22}$). The results are shown in Fig. 2, in which the superconducting gaps are reported as functions of the energy band gap E_g for different values of the total density $a^2 n_{\text{tot}}$ and for different pair-exchange couplings $\lambda_{12} = \lambda_{21}$. In the case of an empty conduction band and a completely filled valence band corresponding to $a^2 n_{\text{tot}} = 2.00$, a QPT to the normal state takes place at a specific quantum critical point (QCP) that occurs when $E_g = E_g^*$. When the carrier concentration in the conduction band is nonzero, the phase transition disappears and superconductivity extends for all values of the band gap E_g . However, the system presents different behaviors if the value of the band gap is smaller or larger of E_g^* . For finite doping, the valence band contributes very weakly to the superconducting state of the system for $E_g > E_g^*$. In this regime, the bands are almost decoupled and the superconducting gaps does not depend on E_g . However, in the case of Fig. 2(c), since the pair-exchange couplings are weak, the conduction band cannot sustain the superconductivity in the valence band and Δ_1 is suppressed. Thus, continuously tuning E_g to higher values will result in $\Delta_1 \ll \Delta_2$ so there is only one significant superconducting gap and one significant condensate. In the other case instead [Fig. 2(d)], the pair-exchange couplings are stronger and Δ_1 is not much suppressed with respect to its

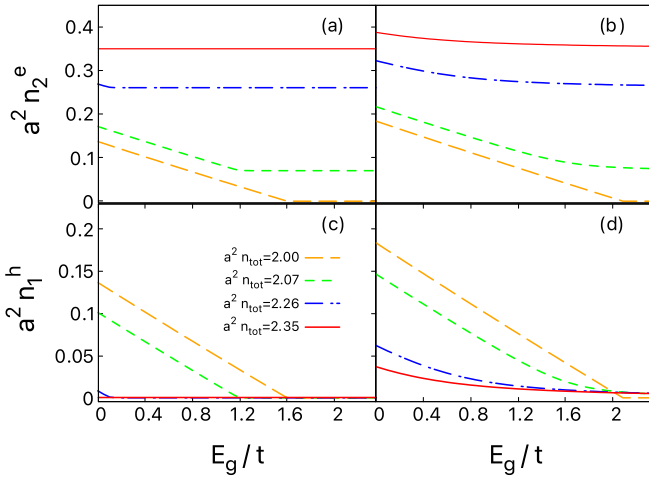


FIG. 3. Electron density $a^2 n_2^e$ (a), (b) in the conduction band and hole density $a^2 n_1^h$ (c), (d) in the valence band as functions of the band gap E_g/t for different values of the total density $a^2 n_{\text{tot}}$, normalized to the area of the unit cell. $\omega_0/t = 20$. The intraband couplings are $\lambda_{11} = 0.23$ and $\lambda_{22} = 0.75$. The pair-exchange couplings are $(\lambda_{12} = \lambda_{21})$: (a), (c) (0.001); (b), (d) (0.1).

initial value, since in these cases the superconductivity in the valence band is sustained by the condensate of the conduction band.

Another interesting feature of this system is that Δ_1 is enhanced for lower values of the total density as long as $E_g < E_g^*$. When $E_g > E_g^*$ instead, the opposite situation occurs. The value of E_g^* at which this behavior takes place depends on the level of filling of the conduction band, shifting to the left when higher total densities are considered, and on the pair-exchange couplings that shifts E_g^* to the right when larger interaction strengths are considered. The reason for the behavior of the superconducting gaps can be found by looking at the densities of particles forming Cooper pairs, which are electrons in the conduction band and holes in the valence band. While the total density is fixed, the density in each band can vary. In this way, the density of particles in the conduction band n_2 is no longer controlled only by doping as for a single band system, there are instead additional particles excited from the valence band. Nevertheless, for larger values of E_g , the gain in the interaction energy due to superconductivity is much smaller than the kinetic energy cost for transferring electrons from the valence band to the conduction band, so very few electrons (compared to the total density of electrons in the valence band) are excited into the conduction band. This behavior is shown in Fig. 3. As one can see for $a^2 n_{\text{tot}} = 2.00$, the hole density in the valence band and the electron density in the conduction band coincide and are monotonically decreasing, both of them vanishing at the QCP $E_g = E_g^*$. This is a sign that superconductivity is due to holes in the valence band and to electrons in the conduction band. In the other cases, the hole density in the valence band is almost zero for $E_g > E_g^*$, while the electron density in the conduction band is approaching the asymptotic value given by the total density minus the density of the filled valence band $a^2 n_2 = a^2 n_{\text{tot}} - 2.00$.

Regarding the single-particle excitation gap E_{ex} in the quasiparticle excitation spectra, in our two-band system the

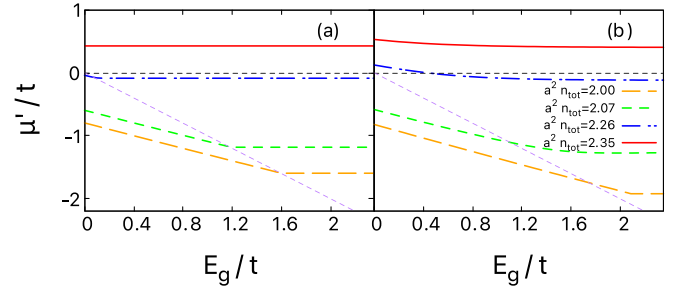


FIG. 4. Shifted chemical potential μ'/t as a function of the band gap E_g/t for $\omega_0/t = 20$. The intraband couplings are $\lambda_{11} = 0.23$ and $\lambda_{22} = 0.75$. The pair-exchange couplings are $(\lambda_{12} = \lambda_{21})$: (a) (0.001), (b) (0.1). The chemical potential μ' is reported for different total densities $a^2 n_{\text{tot}}$. The black and magenta dashed lines correspond to the bottom of the conduction band and the top of the valence band, respectively.

situation is more complex and rich with respect to the single-band case. In the two-band system, there are four branches in the spectrum (two branches coming from the valence band and the other two coming from the conduction band) and E_{ex} can be expressed as

$$E_{\text{ex}} = \min_{\mathbf{k}} \{2E_1(\mathbf{k}), 2E_2(\mathbf{k})\}. \quad (23)$$

In our parameter configuration, this minimum energy is always taken by the single-particle dispersion of the valence band, whose intraband coupling is smaller than the one of the conduction band. Thus, when the chemical potential lies inside the valence band, the excitation gap coincides with twice the superconducting gap in the valence band, $E_{\text{ex}} = 2\Delta_1$, while when the chemical potential lies outside the valence band, the excitation gap results in $E_{\text{ex}} = 2\sqrt{\xi_1(\mathbf{0})^2 + \Delta_1^2}$.

In Fig. 4, the shifted chemical potential $\mu' = \mu + 4t$ is reported as a function of E_g for different total densities $a^2 n_{\text{tot}}$ and different pair-exchange couplings. We have defined a shifted chemical potential to be consistent with the conventional way of observing the crossover, with the BCS regime corresponding to the region in which $\mu' > 0$, while the BEC regime corresponds to the region in which $\mu' < 0$. The corresponding bottom of the conduction band and top of the valence band have been shifted by $4t$ to make them touch at zero energy when $E_g = 0$. This shift does not affect the results, since they depend on the energy difference between the two bands. For higher values of the total density and the pair-exchange couplings, the chemical potential shifts toward higher energies due to the larger number of electrons in the conduction band. In particular, when E_g is increased, in the low-density regime the chemical potential starts deep inside the valence band and then enters the gap between the two bands, meaning that the condensate in the valence band spans a wide region of the BCS-BEC crossover, while the conduction band is always located on the BEC side of the crossover regime or in the BEC regime, depending on whether the chemical potential lies inside the conduction band or not. When $E_g > E_g^*$, the chemical potential acquires a flat dependence and is not modified by E_g , in a similar way to what happens to the superconducting gaps and the densities.

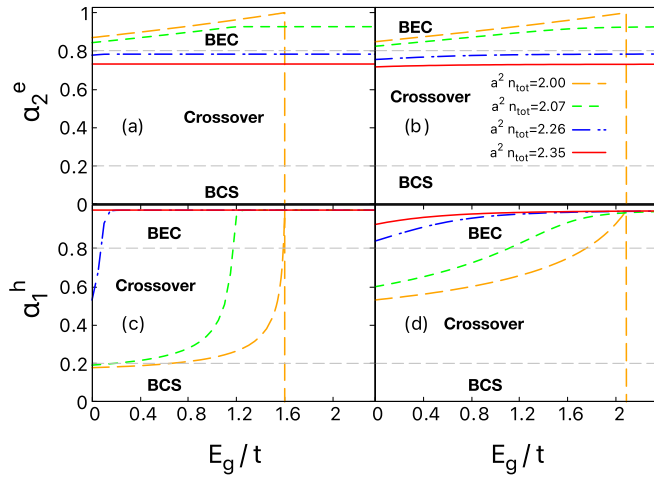


FIG. 5. Condensate fractions in the conduction band α_c^e (a), (b) and in the valence band α_v^h (c), (d) as functions of the band gap E_g/t for $\omega_0/t = 20$. The intraband couplings are $\lambda_{11} = 0.23$ and $\lambda_{22} = 0.75$. The pair-exchange couplings are ($\lambda_{12} = \lambda_{21}$): (a), (c) (0.001); (b), (d) (0.1). The condensate fractions are reported for different total densities $a^2 n_{\text{tot}}$. Thin grey dashed lines correspond to $\alpha = 0.2, 0.8$ from bottom to top.

In Fig. 5, the condensate fraction is shown as a function of E_g for different $a^2 n_{\text{tot}}$ and different pair-exchange couplings. The usual choice of the boundaries between the different pairing regimes has been adopted: For $\alpha < 0.2$, the superconducting state is in the weak-coupling BCS regime; for $0.2 < \alpha < 0.8$, the system is in the crossover regime; for $\alpha > 0.8$, the system is in the strong-coupling BEC regime. Consistent with the information obtained from the chemical potential, in the low-density regime the condensate in the valence band explores the entire BCS-BEC crossover by varying E_g . For the considered pair-exchange interactions [Fig. 5(c)], the valence band condensate is in the BCS regime for small E_g , while larger pair-exchange interactions [Fig. 5(d)] are in the crossover regime. When the energy gap or the total density increases, the valence band condensate enters the BEC regime, with the hole condensate fraction α_v^h approaching unity, indicating that the remaining few holes are all in the condensate. The situation in the conduction band is different, since due to the strong intraband coupling the condensate is always located on the BEC side of the crossover regime or in the BEC regime. In the case $a^2 n_{\text{tot}} = 2.00$, both condensate fractions suddenly drop to zero when $E_g = E_g^*$ due to the QPT.

In Fig. 6, the intrapair coherence length is reported as a function of E_g for different $a^2 n_{\text{tot}}$ and different pair-exchange couplings. Since for low densities and small pair-exchange couplings, the valence band condensate is in the BCS regime [Fig. 6(a)] when E_g is small, ξ_{pair_1} assumes initially larger values with respect to the average interparticle distance l_1 . For larger E_g , the system enters the BEC regime and ξ_{pair_1} becomes much smaller than the average interparticle distance. The valence band condensate goes from the crossover to the BEC regime in a small range of band gap values. This behavior is also observed for larger values of the total density. The conduction band instead, due to the strong intraband

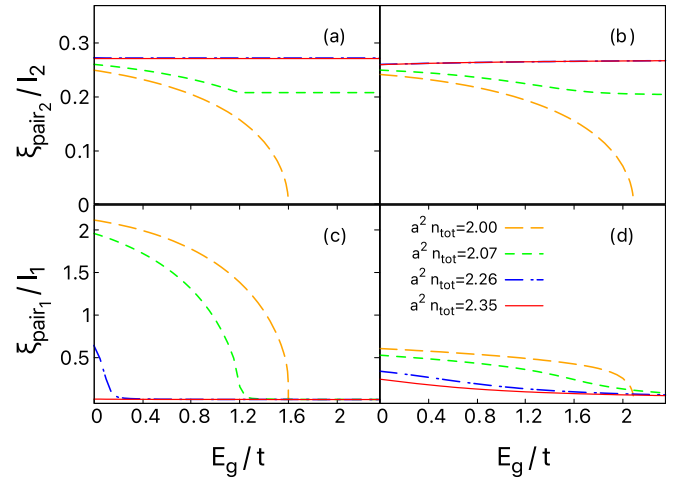


FIG. 6. Intra-pair coherence length ξ_{pair_2}/l_2 for the Cooper pairs of the conduction band (a), (b) and intrapair coherence length ξ_{pair_1}/l_1 for the Cooper pairs of the valence band (c), (d) as functions of the band-gap E_g/t for $\omega_0/t = 20$. The intra-band couplings are $\lambda_{11} = 0.23$ and $\lambda_{22} = 0.75$. The pair-exchange couplings are ($\lambda_{12} = \lambda_{21}$): (a), (c) (0.001), (b), (d) (0.1). The intra-pair coherence lengths ξ_{pair_i}/l_i are reported for different $a^2 n_{\text{tot}}$.

coupling, retains a small value of the intrapair coherence length with respect to the the average interparticle distance l_2 for all considered values of the system density. In this way, we found Cooper pairs of different sizes coexisting in the system for low density and low pair-exchange couplings values, in the regime of small E_g . For the zero doping case, the intrapair coherence length is defined only for $E_g < E_g^*$, since in this regime the system is not superconducting and an intrapair coherence length cannot be defined. The fact that the intrapair coherence length is approaching zero at the QCP in the BEC regime is different from Ref. [35], where giant Cooper pairs are found in the vicinity of the QCP in the BCS side. In this case instead, what we have found is equivalent to the finite-density to zero-density QCP of tightly bound molecules, namely, near the present QCP in the BEC side the pair size is so small that pairs behave as point-like bosons and the system can be described by its bosonic counterpart [43].

In Fig. 7, the order parameter coherence length is reported as a function of E_g for different $a^2 n_{\text{tot}}$ and different pair-exchange couplings. In the case $a^2 n_{\text{tot}} = 2.00$, the soft or critical coherence length ξ_s diverges when the band gap reaches the critical value $E_g = E_g^*$, since the system undergoes a QPT to the insulating state. In the other cases $a^2 n_{\text{tot}} \neq 2.00$, the soft coherence length ξ_s is not diverging, since no QPT occurs in the system for any E_g . In particular, in the cases of $a^2 n_{\text{tot}} = 2.07$ and $a^2 n_{\text{tot}} = 2.26$, the soft coherence length ξ_s shows a maximum in correspondence of the respective $E_g = E_g^*$, showing its memory about the QPT of the valence band condensate, which takes place when the pair-exchange interactions are absent. The increase of $\lambda_{12} = \lambda_{21}$ suppresses the maximum, as shown in Figs. 7(a) and 7(b), since the band condensates become more coupled. In the case of $a^2 n_{\text{tot}} = 2.35$ instead, since the valence band is never superconducting for any E_g when the band condensates are decoupled, there is

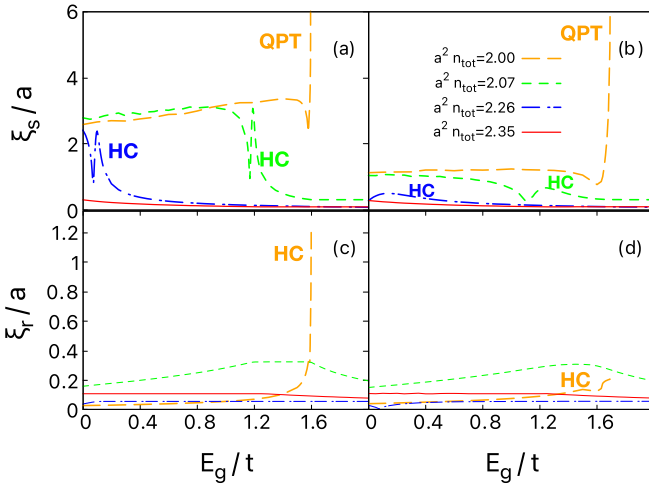


FIG. 7. Soft ξ_s (a), (b) and rigid ξ_r (c), (d) order parameter coherence length, normalized to the lattice constant a , as functions of the band gap E_g/t between the two bands at temperature $T/t = 0.00065$ and for $\omega_0/t = 20$. The intraband couplings are $\lambda_{11} = 0.23$ and $\lambda_{22} = 0.75$. The pair-exchange couplings are ($\lambda_{12} = \lambda_{21}$): (a), (c) (0.001); (b), (d) (0.03). The coherence lengths $\xi_{s,r}$ are reported for different values of the total density $a^2 n_{\text{tot}}$. In the case $a^2 n_{\text{tot}} = 2.00$, (orange dashed line) ξ_r has been rescaled by a factor of 7 (c) and 4.5 (d) to make the plot more visible.

no QPT and no peak. The rigid coherence length ξ_r instead remains finite for all E_g and for all $a^2 n_{\text{tot}}$. Anyway, we find the memory of the QPT that takes place when the conduction band is empty and the valence band is filled ($a^2 n_{\text{tot}} = 2.00$). In this case, in fact, the conduction band also returns to the normal state at $E_g = E_g^*$. Indeed, for zero pair-exchange couplings, the rigid coherence length ξ_r reduces to the coherence length of the conduction band ξ_2 . Even though for finite pair-exchange coupling the coherence length is nondiverging, it encodes the memory of the QPT of the conduction band. Also, the maximum value of the rigid coherence length ξ_r is suppressed by the increase of $\lambda_{12} = \lambda_{21}$ in this case, as shown in Figs. 7(c) and 7(d).

We consider now finite-temperature effects on the critical energy band gap for the case of no doping. The superconducting gaps as functions of temperature for different band gaps are reported in Fig. 8. The superconducting gaps present a nonmonotonic behavior that is very different from the temperature dependence of the gaps in conventional superconductors. The strong enhancement of Δ_2 at finite temperature is due to the thermal excitation of the electrons from the valence band to the conduction band. The enhancement of Δ_1 instead is weaker, since the intraband coupling of the conduction band is larger than the one of the valence band. This behavior becomes more pronounced for larger E_g , especially in the case of Fig. 8(c) in which the system is initially in the normal state for temperatures close to zero, and then becomes superconducting for larger temperatures. This superconducting-normal state reentrant transition that we have found in our two-band system is based on a different mechanism with respect to the

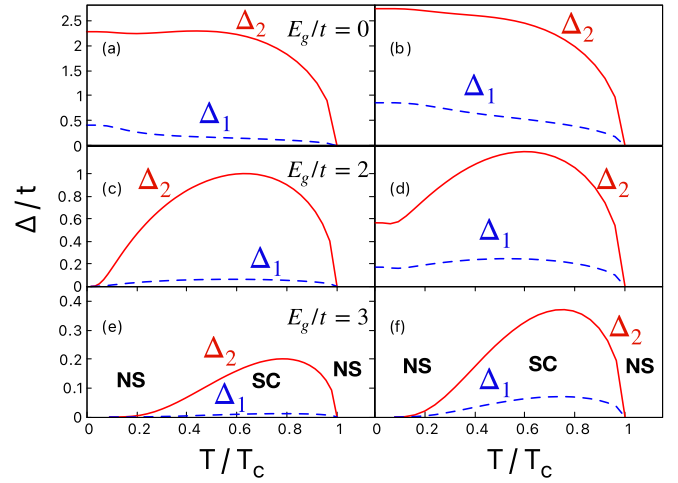


FIG. 8. Superconducting gaps Δ_2/t opening in the conduction band and in the valence band Δ_1/t as functions of temperature T , normalized with respect to the critical temperature T_c , for $a^2 n_{\text{tot}} = 2.00$. The intraband couplings are $\lambda_{11} = 0.23$ and $\lambda_{22} = 0.75$. The pair-exchange couplings are ($\lambda_{12} = \lambda_{21}$): (a), (c), (e) (0.03); (b), (d), (f) (0.1).

reentrant transitions observed in superconductors containing magnetic elements or in granular superconducting systems: In the former, it is attributed to the competition of magnetic ordering and superconductivity and in the latter it is attributed to tunneling barriers effect, while in our valence-conduction band system the thermal excitation of electrons from the valence into the conduction band plays a crucial role. For instance, granular $\text{BaPb}_{0.75}\text{Bi}_{0.25}\text{O}_3$ [44], $\text{Ba}_{0.6}\text{K}_{0.4}\text{BiO}_3$ [45], and Al thin films [46] show a finite resistance appearing when the temperature is lowered in the superconducting state, evidencing a similar character to the reentrant transition that we have found in our system. In granular superconductors consisting of grains of transition metals (W, Mo, Nb, Cr) immersed in a diamondlike carbon-silicon dielectric matrix C-Si-W instead, the reentrant transition manifests as small peaks of resistance, but with the lowering of temperature superconductivity recovered [47]. Among the magnetic rare-earth elements, $\text{HoNi}_2\text{B}_2\text{C}$ and $\text{ErNi}_2\text{B}_2\text{C}$ recover the normal state and then return to the superconducting state again by lowering the temperature, while in $\text{TmNi}_2\text{B}_2\text{C}$ the resistivity shows a continuous recovery towards the normal state and does not show any sign of coming back to the superconducting state [48], with this one being more similar to our system. In Fig. 9, we report the phase diagram T versus E_g for our system. The branch of the phase transition from the superconducting to the normal state corresponding to the reentrant behavior results from the second solution at lower temperatures of the linearized self-consistent equations for the superconducting gaps. From the left panel of Fig. 9, it is clear how the reentrant transition is more pronounced when the intraband couplings are unbalanced ($\lambda_{22} \simeq 3\lambda_{11}$ in the figure), while the reentrance is reduced when the intraband couplings have similar values. This effect also occurs in a less evident manner when the

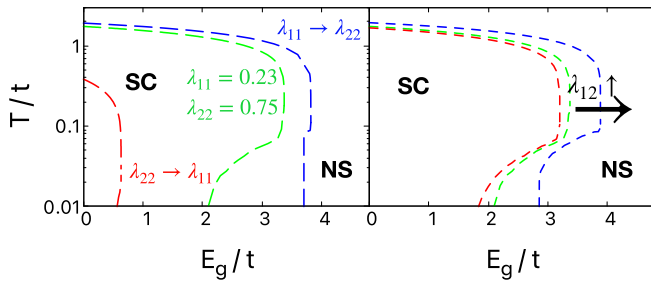


FIG. 9. Phase diagrams in the temperature versus energy band gap plane, for the zero doping case. In the left panel, the red dashed line is for $\lambda_{11} = 0.23$, $\lambda_{22} = 0.4$; the green dashed line is for $\lambda_{11} = 0.23$, $\lambda_{22} = 0.75$; and the blue dashed line is for $\lambda_{11} = 0.65$, $\lambda_{22} = 0.75$. The pair-exchange couplings are the same for all curves, $\lambda_{12} = \lambda_{21} = 0.1$. In the right panel, the pair-exchange couplings from left to right are $\lambda_{12} = \lambda_{21} = 0.03, 0.1, 0.2$, while the intraband couplings are $\lambda_{11} = 0.23$ and $\lambda_{12} = 0.75$.

pair-exchange couplings are increased. Therefore, the most relevant parameter to control the reentrance phenomenon is the intraband coupling.

IV. CONCLUSIONS

We have studied the superconducting properties of a two-band system of electrons, interacting through a separable attractive potential with a large energy cutoff and multiple pairing channels, at a mean-field level. The superconducting state properties are studied by varying the energy gap between the bands. We have considered different levels of filling for the conduction band, while the valence band is always completely filled. When the band gap is modified, the density of electrons in the two bands changes, allowing for the occurrence of a density-induced BCS-BEC crossover. When the pair-exchange couplings are small, the condensate in the valence band remains superconducting but with a strongly suppressed superconducting gap Δ_1 for $E_g > E_g^*$. Therefore, in the regime of small pair-exchange coupling, after E_g^* , there is only one significant superconducting gap and one significant condensate. Interestingly, in this case the soft coherence length present a peak as a memory of the QPT that the valence band condensate undergoes in the absence of pair exchanges. This peak is more pronounced if the pair-exchange couplings are sufficiently weak and disappears for higher values of the pair-exchange couplings. For higher values of λ_{ij} , superconductivity in the valence band is sustained by the condensate in the conduction band. Furthermore, in this regime we have found that superconductivity is enhanced in the valence band for increasing doping as long as $E_g < E_g^*$, while for $E_g > E_g^*$ superconductivity is enhanced for lower doping. We have also found that superconductivity may occur even when no free carriers exist in the conduction band in the normal state at $T = 0$, as soon as the gain in superconducting energy exceeds the cost in producing carriers across the band gap E_g . If the binding energy is larger than the energy band gap, the system becomes unstable under the formation of Cooper pairs and superconductivity emerges. However, there exists a critical value of the energy band gap E_g^* in correspondence of which

the process of creating Cooper pairs is not energetically favorable anymore, at this point a QPT occurs. This QPT is confirmed by the soft coherence length, which is diverging in correspondence to the critical band gap $E_g = E_g^*$. Thus, the ground state is superconducting if $E_g < E_g^*$; insulating if $E_g > E_g^*$. At finite temperature, the value of E_g^* is larger than its zero temperature value because the electrons are thermally excited from the valence band. This situation is responsible for the nonmonotonic behavior of the superconducting gap opening in the conduction band, which is enhanced at low temperatures because of the electrons that jump from the valence band into the conduction band due to thermal excitation. When there is a finite doping in the system, the QPT disappears and superconductivity extends for all E_g . In this case, for $E_g > E_g^*$ the valence band contributes very weakly to the superconducting state, since the hole density becomes almost zero in this regime.

To conclude, we have found that the system explores different regimes of the BCS-BEC crossover by tuning the energy band gap and total density. The valence-band condensate spans the entire BCS-BEC crossover for low enough density by varying the band gap E_g . For larger values of the total density, the condensate of the valence band is very dilute and results in the BEC regime for any E_g . The condensate of the conduction band instead resides in the BEC side of the crossover or completely inside the BEC regime due to the strength of the intraband coupling of electrons in the conduction band. This picture of the BCS-BEC crossover for the system has been found by analyzing the consistent behavior of the chemical potential, the condensate fractions, and the coherence lengths. Moreover, in the case of zero doping and at finite temperature, an interesting type of reentrant superconducting to normal state transition has been numerically discovered for unbalanced intraband couplings, showing that in this configuration superconductivity is assisted instead of being suppressed by increasing temperature. This happens because the electrons in the valence band are able to jump into the conduction band even for larger values of the zero-temperature critical band gap due to thermal excitation, making the superconducting state available for a wider range of E_g when the temperature is higher. Finally, a discussion on the role of random and spatially correlated disorder throughout the BCS-BEC crossover is in order to make a connection with real materials. The effects of disorder are minor in the BCS regime of the crossover when the Fermi surface is well formed and the Anderson's theorem demonstrates that superconducting properties are not modified by nonmagnetic disorder. On the other hand, disorder can lead to an increase of the critical temperature T_c and a widening of the pseudogap energy at T_c in the crossover regime, while on the BEC side of the crossover the presence of disorder favors the collapse of the Fermi surface [49]. Disorder can actually favor the occurrence of pairing correlations, thus changing the statistical properties of the Cooper pairs and enhancing multifractal features of the superconducting order parameter [50,51]. In the regime of the BCS-BEC crossover, many-body correlations due to the interplay between disorder and superconducting pair fluctuations and spatial correlations may cooperate to enhance superconductivity, making it more robust and less

sensitive to the disorder. In our system, the increase of pair correlations and the pseudogap due to disorder can be taken into account by renormalization of the energy band gap E_g , which modifies in a quantitative way, but not qualitatively, the phase and crossover diagrams. A quantitative analysis of the effects of disorder on our conclusions will be the subject of future investigations.

ACKNOWLEDGMENTS

We are grateful to Tiago Saraiva (HSE-Moscow) and Hiroyuki Tajima (University of Tokyo) for interesting discussions and a critical reading of the paper. G.M. acknowledges INFN for financial support of his Ph.D. grant. This work has been partially supported by PNRR MUR Project No. PE0000023-NQSTI.

-
- [1] M. V. Milošević and A. Perali, Emergent phenomena in multicomponent superconductivity: An introduction to the focus issue, *Supercond. Sci. Technol.* **28**, 060201 (2015).
- [2] D. M. Eagles, Possible pairing without superconductivity at low carrier concentrations in bulk and thin-film superconducting semiconductors, *Phys. Rev.* **186**, 456 (1969).
- [3] A. J. Leggett, in *Modern Trends in the Theory of Condensed Matter*, edited by A. Pekelski and J. Przystawa (Springer-Verlag, Berlin, 1980), p. 13.
- [4] Q. Chen, J. Stajic, S. Tan, and K. Levin, BCS-BEC crossover: From high temperature superconductors to ultracold superfluids, *Phys. Rep.* **412**, 1 (2005).
- [5] G. C. Strinati, P. Pieri, G. Röpke, P. Schuck, and M. Urban, The BCS-BEC crossover: From ultra-cold Fermi gases to nuclear systems, *Phys. Rep.* **738**, 1 (2018).
- [6] A. A. Shanenko, M. D. Croitoru, A. Vagov, and F. M. Peeters, Giant drop in the Bardeen-Cooper-Schrieffer coherence length induced by quantum size effects in superconducting nanowires, *Phys. Rev. B* **82**, 104524 (2010).
- [7] Y. Chen, A. A. Shanenko, A. Perali, and F. M. Peeters, Superconducting nanofilms: Molecule-like pairing induced by quantum confinement, *J. Phys.: Condens. Matter* **24**, 185701 (2012).
- [8] D. Innocenti, N. Poccia, A. Ricci, A. Valletta, S. Caprara, A. Perali, and A. Bianconi, Resonant and crossover phenomena in a multiband superconductor: Tuning the chemical potential near a band edge, *Phys. Rev. B* **82**, 184528 (2010).
- [9] M. V. Mazziotti, A. Valletta, G. Campi, D. Innocenti, A. Perali, and A. Bianconi, Possible Fano resonance for high-Tc multi-gap superconductivity in p-Terphenyl doped by K at the Lifshitz transition, *Europhys. Lett.* **118**, 37003 (2017).
- [10] L. Salasnich, A. A. Shanenko, A. Vagov, J. Albino Aguiar, and A. Perali, Screening of pair fluctuations in superconductors with coupled shallow and deep bands: A route to higher-temperature superconductivity, *Phys. Rev. B* **100**, 064510 (2019).
- [11] H. Tajima, Y. Yerin, A. Perali, and P. Pieri, Enhanced critical temperature, pairing fluctuation effects, and BCS-BEC crossover in a two-band Fermi gas, *Phys. Rev. B* **99**, 180503(R) (2019).
- [12] H. Tajima, Y. Yerin, P. Pieri, and A. Perali, Mechanisms of screening or enhancing the pseudogap throughout the two-band Bardeen-Cooper-Schrieffer to Bose-Einstein condensate crossover, *Phys. Rev. B* **102**, 220504(R) (2020).
- [13] T. T. Saraiva, P. J. F. Cavalcanti, A. Vagov, A. S. Vasenko, A. Perali, L. Dell'Anna, and A. A. Shanenko, Multiband Material with a Quasi-1D Band as a Robust High-Temperature Superconductor, *Phys. Rev. Lett.* **125**, 217003 (2020).
- [14] T. T. Saraiva, L. I. Baturina, and A. A. Shanenko, Robust superconductivity in quasi-one-dimensional multiband materials, *J. Phys. Chem. Lett.* **12**, 11604 (2021).
- [15] A. A. Shanenko, T. T. Saraiva, A. Vagov, A. S. Vasenko, and A. Perali, Suppression of fluctuations in a two-band superconductor with a quasi-one-dimensional band, *Phys. Rev. B* **105**, 214527 (2022).
- [16] A. M. Gabovich and A. I. Voitenko, Model for the coexistence of d -wave superconducting and charge-density-wave order parameters in high-temperature cuprate superconductors, *Phys. Rev. B* **80**, 224501 (2009).
- [17] A. M. Gabovich and A. I. Voitenko, Coexistence of charge density waves and d -wave superconductivity in cuprates. Sharing of the Fermi surface, *Z. Kristallogr.* **225**, 492 (2010).
- [18] R. Arpaia, S. Caprara, R. Fumagalli, G. De Vecchi, Y. Y. Peng, E. Andersson, D. Betto, G. M. De Luca, N. B. Brookes, F. Lombardi *et al.*, Dynamical charge density fluctuations pervading the phase diagram of a Cu-based high-Tc superconductor, *Science* **365**, 906 (2019).
- [19] A. Perali, C. Castellani, C. Di Castro, and M. Grilli, d -wave superconductivity near charge instabilities, *Phys. Rev. B* **54**, 16216 (1996).
- [20] K. Rossnagel, On the origin of charge density waves in select layered transition-metal dichalcogenides, *J. Phys.: Condens. Matter* **23**, 213001 (2011).
- [21] A. H. Castro Neto, Charge Density Wave, Superconductivity, and Anomalous Metallic Behavior in 2D Transition Metal Dichalcogenides, *Phys. Rev. Lett.* **86**, 4382 (2001).
- [22] T. Kiss, T. Yokoya, A. Chainani, S. Shin, T. Hanaguri, M. Nohara, and H. Takagi, Charge-order-maximized momentum-dependent superconductivity, *Nat. Phys.* **3**, 720 (2007).
- [23] M. Calandra, I. I. Mazin, and F. Mauri, Effect of dimensionality on the charge-density wave in few-layer 2H-NbSe₂, *Phys. Rev. B* **80**, 241108(R) (2009).
- [24] Y. Ge and A. Y. Liu, Effect of dimensionality and spin-orbit coupling on charge-density-wave transition in 2H-TaSe, *Phys. Rev. B* **86**, 104101 (2012).
- [25] M. M. Ugeda, A. J. Bradley, Y. Zhang, S. Onishi, Y. Chen, W. Ruan, C. Ojeda-Aristizabal, H. Ryu, M. T. Edmonds, H. Tsai *et al.*, Characterization of collective ground states in single-layer NbSe₂, *Nat. Phys.* **12**, 92 (2016).
- [26] Y. Cao, A. Mishchenko, G. L. Yu, E. Khestanova, A. P. Rooney, E. Prestat, A. V. Kretinin, P. Blake, M. B. Shalom, C. Woods *et al.*, Quality heterostructures from two-dimensional crystals unstable in air by their assembly in inert atmosphere, *Nano Lett.* **15**, 4914 (2015).
- [27] CS. Lian, C. Heil, X. Liu, C. Si, F. Giustino, and W. Duan, Coexistence of superconductivity with enhanced charge-density

- wave order in the two-dimensional limit of TaSe, *J. Phys. Chem. Lett.* **10**, 4076 (2019).
- [28] J.-F. Ge, Z.-L. Liu, C. Liu, C.-L. Gao, D. Qian, Q.-K. Xue, Y. Liu, and J.-F. Jia, Superconductivity above 100 K in single-layer FeSe films on doped SrTiO₃, *Nat. Mater.* **14**, 285 (2015).
- [29] H. Lin, W. Huang, G. Rai, Y. Yin, L. He, Q. K. Xue, S. Haas, S. Kettemann, X. Chen, and S. H. Ji, Real-space BCS-BEC crossover in FeSe monolayers, *Phys. Rev. B* **107**, 104517 (2023).
- [30] H. Zhou, L. Holleis, Y. Saito, L. Cohen, W. Huynh, C. L. Patterson, F. Yang, T. Taniguchi, K. Watanabe, and A. F. Young, Isospin magnetism and spin-polarized superconductivity in Bernal bilayer graphene, *Science* **375**, 774 (2022).
- [31] P. A. Pantaleón, A. Jimeno-Pozo, H. Sainz-Cruz, V. T. Phong, T. Cea, and F. Guinea, Superconductivity and correlated phases in non-twisted bilayer and trilayer graphene, *Nat. Rev. Phys.* (2023), doi: 10.1038/s42254-023-00575-2.
- [32] Y. Zhang, R. Polski, A. Thomson, . Lantagne-Hurtubise, C. Lewandowski, H. Zhou, K. Watanabe, T. Taniguchi, J. Alicea, and S. Nadj-Perge, Enhanced superconductivity in spin-orbit proximitized bilayer graphene, *Nature (London)* **613**, 268 (2023).
- [33] S. Conti, A. Perali, F. M. Peeters, and D. Neilson, Multicomponent Electron-Hole Superfluidity and the BCS-BEC Crossover in Double Bilayer Graphene, *Phys. Rev. Lett.* **119**, 257002 (2017).
- [34] P. Nozières and F. Pistolesi, From semiconductors to superconductors: A simple model for pseudogaps, *Eur. Phys. J. B* **10**, 649 (1999).
- [35] Y. Yerin, H. Tajima, P. Pieri, and A. Perali, Coexistence of giant Cooper pairs with a bosonic condensate and anomalous behavior of energy gaps in the BCS-BEC crossover of a two-band superfluid Fermi gas, *Phys. Rev. B* **100**, 104528 (2019).
- [36] N. Andrenacci, A. Perali, P. Pieri, and G. C. Strinati, Density-induced BCS to Bose-Einstein crossover, *Phys. Rev. B* **60**, 12410 (1999).
- [37] Y. R. Shi, W. Zhang, and C. A. R. Sá de Melo, The evolution from BCS to Bose pairing in two-band superfluids: Quantum phase transitions and crossovers by tuning band offset and interactions, *Europhys. Lett.* **139**, 36004 (2022).
- [38] T. Örd, K. Rago, and A. Vargunin, Critical and non-critical coherence lengths in a two-band superconductor, *J. Supercond. Novel Magn.* **25**, 1351 (2012).
- [39] A. Guidini and A. Perali, Band-edge BCS-BEC crossover in a two-band superconductor: Physical properties and detection parameters, *Supercond. Sci. Technol.* **27**, 124002 (2014).
- [40] A. A. Vargas-Paredes, A. A. Shanenko, A. Vagov, M. V. Milosevic, and A. Perali, Crossband versus intraband pairing in superconductors: Signatures and consequences of the interplay, *Phys. Rev. B* **101**, 094516 (2020).
- [41] P. López Ríos, A. Perali, R. J. Needs, and D. Neilson, Evidence from Quantum Monte Carlo Simulations of Large-Gap Superfluidity and BCS-BEC Crossover in Double Electron-Hole Layers, *Phys. Rev. Lett.* **120**, 177701 (2018).
- [42] D. Neilson, A. Perali, and A. R. Hamilton, Excitonic superfluidity and screening in electron-hole bilayer systems, *Phys. Rev. B* **89**, 060502(R) (2014).
- [43] K. Furutani, A. Perali, and L. Salasnich, Berezinskii-Kosterlitz-Thouless phase transition with Rabi coupled bosons, *Phys. Rev. A* **107**, L041302 (2023).
- [44] T. H. Lin, X. Y. Shao, M. K. Wu, P. H. Hor, X. C. Jin, and C. W. Chu, Observation of a reentrant superconducting resistive transition in granular BaPb_{0.75}Bi_{0.25}O₃ superconductor, *Phys. Rev. B* **29**, 1493 (1984).
- [45] U. Welp, W. K. Kwok, G. W. Crabtree, H. Claus, K. G. Vandervoort, B. Dabrowski, A. W. Mitchell, D. R. Richards, D. T. Mark, and D. G. Hinks, The upper critical field of Ba_{1-x}K_xBiO₃, *Physica C* **156**, 27 (1988).
- [46] T. Suzuki, T. Tsuboi, H. Takaki, T. Nizusaki, and T. Kusumoto, Reentrant superconductivity in aluminum thin films under high magnetic field, *J. Phys. Soc. Jpn.* **52**, 981 (1983).
- [47] S. M. Chudinov, G. Mancini, M. Minestrini, R. Natali, S. Stizza, and A. Bozhko, Critical current in granular superconductor C-Si-W with peak-type re-entrant superconductivity, *J. Phys.: Condens. Matter* **14**, 193 (2002).
- [48] H. Eisaki, H. Takagi, R. J. Cava, B. Batlogg, J. J. Krajewski, W. F. Peck, Jr., K. Mizuhashi, J. O. Lee, and S. Uchida, Competition between magnetism and superconductivity in rare-earth nickel boride carbides, *Phys. Rev. B* **50**, 647(R) (1994).
- [49] F. Palestini and G. C. Strinati, Systematic investigation of the effects of disorder at the lowest order throughout the BCS-BEC crossover, *Phys. Rev. B* **88**, 174504 (2013).
- [50] V. D. Neverov, A. E. Lukyanov, A. V. Krasavin, A. Vagov, and M. D. Croitoru, Correlated disorder as a way towards robust superconductivity, *Commun. Phys.* **5**, 177 (2022).
- [51] M. D. Croitoru, A. A. Shanenko, A. Vagov, A. S. Vasenko, M. V. Milosevic, V. M. Axt, and F. M. Peeters, Influence of disorder on superconducting correlations in nanoparticles, *J. Supercond. Nov. Magn.* **29**, 605 (2016).